

# Characterization of thin film CO<sub>2</sub> ice through the infrared $\nu_1 + \nu_3$ combination mode

Jiao He,<sup>\*</sup> Gianfranco Vidali,<sup>†</sup>

*Physics Department, Syracuse University, Syracuse, NY 13244, USA*

Accepted XXX. Received YYY; in original form ZZZ

## ABSTRACT

Carbon dioxide is abundant in ice mantles of dust grains; some is found in the pure crystalline form as inferred from the double peak splitting of the bending profile at about 650 cm<sup>-1</sup>. To study how CO<sub>2</sub> segregates into the pure form from water-rich mixtures of ice mantles and how it then crystallizes, we used Reflection Absorption InfraRed Spectroscopy (RAIRS) to study the structural change of pure CO<sub>2</sub> ice as a function of both ice thickness and temperature. We found that the  $\nu_1 + \nu_3$  combination mode absorption profile at 3708 cm<sup>-1</sup> provides an excellent probe to quantify the degree of crystallinity in CO<sub>2</sub> ice. We also found that between 20 and 30 K, there is an ordering transition that we attribute to reorientation of CO<sub>2</sub> molecules, while the diffusion of CO<sub>2</sub> becomes significant at much higher temperatures. In the formation of pure crystalline CO<sub>2</sub> in ISM ices, the rate limiting process is the diffusion/segregation of CO<sub>2</sub> molecules in the ice instead of the phase transition from amorphous to crystalline after clusters/islands of CO<sub>2</sub> are formed.

**Key words:** methods: laboratory: solid state – infrared: ISM – ISM: molecules – ISM: evolution – solid state: volatile

## 1 INTRODUCTION

CO<sub>2</sub>, along with H<sub>2</sub>O and CO, is the main component of the ice mantle covering interstellar dust grains in molecular clouds. In space, solid CO<sub>2</sub> is observed in the mid-infrared by the bending mode ( $\nu_2$ ) at  $\sim 650$  cm<sup>-1</sup> (Gerakines et al. 1999; Pontoppidan et al. 2008; Ioppolo et al. 2013; Noble et al. 2013), the asymmetrical stretching mode ( $\nu_3$ ) at  $\sim 2350$  cm<sup>-1</sup> (Gerakines et al. 1999; Nummelin et al. 2001; Noble et al. 2013), as well as the combination modes  $\nu_1 + \nu_3$  at 3708 cm<sup>-1</sup> and  $2\nu_2 + \nu_3$  at 3600 cm<sup>-1</sup> (Gerakines et al. 1999; Keane et al. 2001). <sup>13</sup>CO<sub>2</sub> can also be observed via the  $\nu_3$  mode at  $\sim 2280$  cm<sup>-1</sup> (de Graauw et al. 1996; Boogert et al. 2000). The symmetric stretch  $\nu_1$  is IR inactive. The abundance of solid CO<sub>2</sub> with respect to H<sub>2</sub>O ice ranges from 5% to 40%, with a median in the 20–30% range, in star formation regions (Boogert et al. 2015; Yamagishi et al. 2015). Because the  $\nu_3$  mode is intense and is often saturated, the  $\nu_2$  mode is often used instead to study the abundance and the physical and chemical environment of solid state CO<sub>2</sub>. Pontoppidan et al. (2008) did a comprehensive survey of the  $\nu_2$  mode of CO<sub>2</sub> in various young stellar objects (YSOs) and found that the

$\nu_2$  absorption profile can be separated into a few components representing different chemical and physical environments for CO<sub>2</sub>. Most interestingly, the double peak splitting of the bending mode—the so-called Davydov splitting (Davydov & Sardaryan 1962)—for pure crystalline CO<sub>2</sub> is found in many lines of sight (Pontoppidan et al. 2008; Ioppolo et al. 2013; Noble et al. 2013). To use the double peak splitting as a thermal history probe, it is crucial to study in the laboratory how CO<sub>2</sub> segregates into patches of pure CO<sub>2</sub> and then crystallizes. The segregation of CO<sub>2</sub> from CO<sub>2</sub>:H<sub>2</sub>O:CH<sub>3</sub>OH or CO<sub>2</sub>:H<sub>2</sub>O mixtures has been studied in several prior works (Sandford & Allamandola 1990; Ehrenfreund et al. 1998, 1999; Gerakines et al. 1999; Palumbo & Baratta 2000; Hodyss et al. 2008; Ioppolo et al. 2013; Isokoski et al. 2014; Cooke et al. 2016) using transmission FTIR spectroscopy. In these studies, and in the IR studies of pure CO<sub>2</sub> ice (see Kataeva et al. (2015) and references cited therein) the ice is much thicker than that of actual ice mantles. It is known that crystallization is characterized by long range order in the solid; in thin films, it depends on the thickness, with the thinner films often being amorphous or partially amorphous with nanocrystals (Loerting et al. 2009). It is more realistic to study the segregation and crystallization in the thickness range comparable with the thickness of ice mantles (less than a few tens of a monolayer (ML)) in the ISM. However, thin films transmis-

\* E-mail: jhe08@syr.edu

† E-mail: gvidali@syr.edu

sion spectroscopy is not sensitive enough to give data with high enough signal to noise ratio. Reflection Absorption InfraRed Spectroscopy (RAIRS) provides a more sensitive alternative to study the segregation and crystallization of CO<sub>2</sub> in thin film ice mixtures, although in general RAIRS spectra has different absorption profile than transmission spectra (Baratta & Palumbo 1998). Öberg et al. (2009) used RAIRS and adopted a more realistic thickness (< 40 ML) of CO<sub>2</sub>:H<sub>2</sub>O mixture to quantify the segregation of CO<sub>2</sub>. They found that segregation of CO<sub>2</sub> becomes significant between 50 and 60 K. Most recently, He et al. (2017) measured the binding energy of CO<sub>2</sub> on water ice and on CO<sub>2</sub> ice, and found that the former is weaker than the latter. Therefore with enough thermal energy CO<sub>2</sub> is more likely to bind to other CO<sub>2</sub> molecules to form clusters instead of binding to water. He et al. (2017) obtained the diffusion energy barrier of CO<sub>2</sub> on the surface of compact amorphous solid water. On a laboratory time scale the diffusion becomes significant at above 60 K, which is in agreement with the temperature found in prior studies of the segregation of CO<sub>2</sub> from CO<sub>2</sub>:H<sub>2</sub>O mixtures (eg., Hodyss et al. 2008; Öberg et al. 2009).

While the segregation of CO<sub>2</sub> in water-based mixtures has been studied by several groups, fewer details are available of the crystallization process of pure CO<sub>2</sub> ice at low temperature. Furthermore, there is some disagreement on the results and their interpretation. Escribano et al. (2013) used theoretical modeling and laboratory measurements using both RAIRS and transmission spectroscopy to study the crystallization of pure CO<sub>2</sub> ice. They found that even for CO<sub>2</sub> ice deposited when the substrate is at 8 K, as long as the ice film is not too thin, the ice is partly crystalline. They also found that when an amorphous CO<sub>2</sub> ice is heated up to 25 K, it becomes crystalline. From 25 K to the desorption temperature, the ice structure does not change, as inferred from the fact that there is no change in the infrared spectra in this temperature range. This is in contradiction with Gerakines & Hudson (2015) and Isokoski et al. (2013). Isokoski et al. (2013) measured high resolution transmission FTIR spectra of pure CO<sub>2</sub> ice deposited at 15 K as well as during heating up, and found that the  $\nu_2$  mode double peak and the combination modes  $\nu_1 + \nu_3$  and  $2\nu_2 + \nu_3$  become narrower and sharper during heating up from 15 K to 75 K. This indicates that the ordering in the ice changes during heating up. Gerakines & Hudson (2015) found that CO<sub>2</sub> ice deposited at 10 K at the rate of 0.1  $\mu\text{m/hr}$ , or about 200 times slower than in Isokoski et al. (2013), does not show any splitting in the bending mode. They claimed that the missing of splitting is attributed to the fact that their CO<sub>2</sub> ice is amorphous. This lack of splitting in Gerakines & Hudson (2015) disagrees with both Escribano et al. (2013) and Isokoski et al. (2013). Since these three groups used different thickness of CO<sub>2</sub> ice, it remains a question whether the difference among them is due to the difference in ice thickness and/or deposition rate (Escribano et al. (2013) used a slightly slower deposition rate than Gerakines & Hudson (2015)). In this work we study systematically how the CO<sub>2</sub> ice crystallization depends on both ice thickness and temperature. We also look for all signatures of CO<sub>2</sub> ice crystallization other than the splitting of bending mode, hoping to find alternative probes of CO<sub>2</sub> crystallinity.

## 2 EXPERIMENTAL SETUP

The experiments were carried out in a ultrahigh vacuum (UHV) setup located at Syracuse University. A base pressure of  $2 \times 10^{-10}$  torr can be obtained routinely. At the center of the chamber there is a gold coated copper disk (the sample) attached to the cold tip of a liquid helium cryostat. A Lakeshore 336 temperature controller with a calibrated silicone diode and a resistance heater were used to measure and control the temperature in the range of 8 – 500 K with an accuracy better than 50 mK. CO<sub>2</sub> gas was deposited onto the sample disk from the background via a UHV precision leak valve. A stepper motor controlled by a LabVIEW program was used to drive the leak valve. The deposition dose was calculated by the integration of pressure over time, assuming 1 Langmuir (1 L,  $1 \times 10^{-6}$  torr·s) of exposure is equivalent to 1 monolayer (ML). Later we use ML and L interchangeably. It is assumed that at a deposition temperature of 10 K the sticking of CO<sub>2</sub> is unity (He et al. 2016), and the pressure at the ionization pressure gauge is the same as that in front of the sample. The standard gas correction factor for CO<sub>2</sub> has been taken into account when calculating the deposition dose. With the automated leak valve, the deposition rate and dose can be controlled to *relative* uncertainty less than 3%. The main uncertainty in thickness comes from the pressure reading of the ion gauge. A systematic error as much as 30% is possible in this type of gauges. For experiments in this work, a CO<sub>2</sub> deposition rate of 4 L/minute was adopted except for the deposition of water and CO<sub>2</sub> mixture. The following thicknesses were attempted: 1, 2, 5, 10, 15, 20, 30 L. After deposition at 10 K, the sample was heated up to 100 K at a rate of 0.1 K/s to desorb the CO<sub>2</sub> ice (Temperature Programmed Desorption). The infrared spectra of the CO<sub>2</sub> ice was monitored by a Nicolet 6700 Fourier Transform InfraRed (FTIR) spectrometer in the Reflection Absorption InfraRed Spectroscopy (RAIRS) setup with an incidence angle of 78 degrees. The FTIR collects and averages 7 spectra from 600  $\text{cm}^{-1}$  to 4000  $\text{cm}^{-1}$  at a resolution of 1  $\text{cm}^{-1}$  every 10 seconds, both during deposition and during Temperature Programmed Desorption (TPD).

## 3 RESULTS AND ANALYSIS

We deposited 1, 2, 5, 10, 15, 20, and 30 L of CO<sub>2</sub> onto the gold surface at 10 K, and then heated up the sample from 10 K to 100 K with a ramp rate of 0.1 K/s. The asymmetrical stretching mode ( $\nu_3$ ) absorption spectra for all these thicknesses, normalized to the maximum of all the spectra for the same thickness during TPD, are shown in Fig. 1. Fig. 2 shows the absorption spectra during TPD at selected temperatures for selected thicknesses (30, 15, 5, and 2 L). The following vibrational modes are shown:  $\nu_1 + \nu_3$  mode at 3708  $\text{cm}^{-1}$ ,  $2\nu_2 + \nu_3$  mode at 3600  $\text{cm}^{-1}$ , asymmetrical stretching mode  $\nu_3$  at  $\sim 2380$   $\text{cm}^{-1}$ ,  $\nu_3$  mode for <sup>13</sup>CO<sub>2</sub> at  $\sim 2280$   $\text{cm}^{-1}$ , bending mode  $\nu_2$  at  $\sim 675$   $\text{cm}^{-1}$ . For  $\nu_3$  and  $\nu_2$  modes, the position of the absorption peaks are blue shifted respect to typical spectra measured in transmission. This is due to the splitting of transverse optical (TO) and longitudinal optical (LO) modes. In RAIRS measurement, usually the LO mode is seen, while in transmission setup at normal incidence only TO mode is excited. For polycrystalline

films, in the reflection mode at normal incidence, a small LO peak is seen as well (Kataeva et al. 2015). The LO and TO modes are present both in amorphous and crystalline solids (Berreman 1963).

We first analyze the  $\nu_3$  mode. In Fig. 2 the second column shows the  $\nu_3$  profile for different temperatures. For all the thicknesses, at the lowest temperature the peak is centered at below  $2380\text{ cm}^{-1}$ , typical of LO mode of disordered CO<sub>2</sub>. Depending on the thickness, at different temperatures the peak blue shifts to  $2381\text{ cm}^{-1}$ , which is the typical position for crystalline CO<sub>2</sub> LO mode (eg., Escribano et al. 2013). As seen in Fig. 1, for 30 L of CO<sub>2</sub>, the first change happens at  $25 \pm 2\text{ K}$ . In thinner ices, this temperature at which there is a change is higher. For 1 L of CO<sub>2</sub>, it is at  $\sim 50\text{ K}$ . For the 30 L and 20 L ices, at above  $\sim 60\text{ K}$  the peak becomes much narrower and the red wing almost disappears. This indicates the formation of long-range order (complete crystallization), as confirmed by the behavior of the  $\nu_1 + \nu_3$  combination mode to be discussed below. The sensitivity to the macroscopic environment of the  $\nu_1 + \nu_3$  combination mode was noted before for nanoparticles (Bauerecker 2005). At the same time, the overall peak area of  $\nu_3$  becomes much smaller. This can be explained if the orientation of CO<sub>2</sub> molecules in the crystal are in a configuration that lowers the LO absorption. If we assume in the amorphous phase the average angle between the linear CO<sub>2</sub> molecules and the surface normal is 45 degrees, in the crystalline form this angle is likely to be smaller than 45 degrees, and the LO mode (which excite vibration mode in the normal direction of the substrate surface) of asymmetrical stretching becomes less intense. At the same time we should expect to see an increase in TO mode absorption. Indeed, Fig. 3 shows the increase in TO mode absorption at  $2343\text{ cm}^{-1}$  at  $\sim 60\text{ K}$ . In the RAIRS, TO mode absorption is usually much weaker than LO because TO mode cancels out at the metal surface if the incident angle is close to 90 degrees. Another dramatic change happens above 80 K during the desorption of CO<sub>2</sub> ice. The peak red shifts from  $\sim 2381\text{ cm}^{-1}$  to lower than  $2380\text{ cm}^{-1}$ , and it broadens. This may be because the symmetry is broken and the ice becomes disordered again, due to the rapid movement of CO<sub>2</sub> molecules during desorption.

In other vibration modes, there are also significant changes accompanying the structural changes. In the  $\nu_2$  LO mode, amorphous CO<sub>2</sub> shows a peak at  $\sim 676\text{ cm}^{-1}$ ; as the ice crystallizes, it blue shifts to  $\sim 679\text{ cm}^{-1}$ . The presence of the naturally occurring isotopic impurity <sup>13</sup>CO<sub>2</sub> provides another powerful marker of the morphology of the film. The  $\nu_3$  mode of <sup>13</sup>CO<sub>2</sub> shows a change from a broad band to a narrow peak at the same temperature of the onset of crystallization that was mentioned above about the  $\nu_3$  mode of <sup>12</sup>CO<sub>2</sub>. Because of the low temperature at the transition ( $\sim 25\text{ K}$  and higher for thinner films) there is no diffusion at the laboratory time scale. Therefore, single <sup>12</sup>CO<sub>2</sub> molecules remain in place, but their environment changes, and this is reflected by the sharpening of the  $\nu_3$  mode. The peak sharpens with increasing degree of crystallinity while the position remains the same at  $2283\text{ cm}^{-1}$ . The combination modes  $\nu_1 + \nu_3$  and  $2\nu_2 + \nu_3$  have the same shape and their magnitudes are proportional. In the ice deposited at low temperature and especially for the thinner films, the combination modes show a broad profile, as expected for an amorphous solid. Here we use the word amorphous loosely, since there

is no direct information on the degree of ordering of the deposit. As an intermediate range order (Price 1996) structure forms, a sharp component shows up, and becomes more pronounced as longer range order is formed. The degree of crystallinity is strictly positively related to the magnitude of the sharp component. We suggest that these combination modes are excellent probe of CO<sub>2</sub> ice crystallinity because they are very pronounced and easy to separate from the broad amorphous component.

Singling out one sharp component is numerically much easier than singling out a double peak. Another advantage of using the combination modes as a crystallinity probe is that they show the same behavior in both transmission and RAIRS spectra (Bauerecker 2005). On the surface of dust grains the combination modes of CO<sub>2</sub> can also be directly compared with RAIRS/transmission measurements without grain shape corrections. To study the segregation of CO<sub>2</sub> in ice mantle, thin ice layers are preferred and RAIRS is more sensitive for such measurement. The  $\nu_2$  and  $\nu_3$  modes in RAIRS are dramatically different from the transmission spectra. Combination modes provide a consistent profile regardless of the geometry of laboratory setup. The coincidence of sharp combination modes and bending mode splitting in transmission spectra has been observed in prior studies (Ehrenfreund et al. 1998; Hodyss et al. 2008), which verifies the validity of using combination modes as indication of crystallization, and also supports that this indication of crystallization applies to transmission spectra as well.

Now we show how the  $\nu_1 + \nu_3$  mode can be used as a probe to study in detail the crystallization of pure CO<sub>2</sub> ice. The  $\nu_1 + \nu_3$  absorption peak can be fit using two components, one sharp and narrow component centered at  $3708\text{ cm}^{-1}$  best fitted with a Lorentzian distribution with  $\gamma = 0.7\text{ cm}^{-1}$ , one broad component fitted with a Gaussian distribution with  $\sigma > 4\text{ cm}^{-1}$ . The Lorentzian component is the signature of crystalline CO<sub>2</sub> while the Gaussian component represents amorphous (or disordered) CO<sub>2</sub> ice. In a single crystalline CO<sub>2</sub> ice only the Lorentzian component can be seen while in the other extreme, fully amorphous CO<sub>2</sub> ice has only a broad Gaussian component. A typical fitting is shown in Fig. 4. Fig. 5 shows the area of both components during the deposition of the 30 L of CO<sub>2</sub> ice when the substrate is at 10 K. Below 10 L the ice is amorphous. As the thickness increases further the crystalline component emerges. This suggests that the underlying polycrystalline/amorphous gold surface may affect the growth of crystalline CO<sub>2</sub> ice. An alternative explanation is that partial crystallization requires at least intermediate range order, and too thin a film at 10 K can not form the intermediate range order at 10 K. The result in Fig. 4 can be extended to thicker ices. Isokoski et al. (2013) deposited 3000 ML of CO<sub>2</sub> when the substrate was at 15 K, and the ice is polycrystalline, which agrees qualitatively with Fig. 4.

In order to better quantify the crystallinity, we define a new parameter—degree of crystallinity (*DOC*) as:

$$DOC = \frac{A_{crystalline}}{A_{crystalline} + A_{amorphous}} \quad (1)$$

where  $A_{crystalline}$  and  $A_{amorphous}$  are the absorption strength of the Lorentzian component and Gaussian component, respectively. Fig. 6 shows the *DOC* as a function of temperature during TPD for different thickness CO<sub>2</sub> ices.

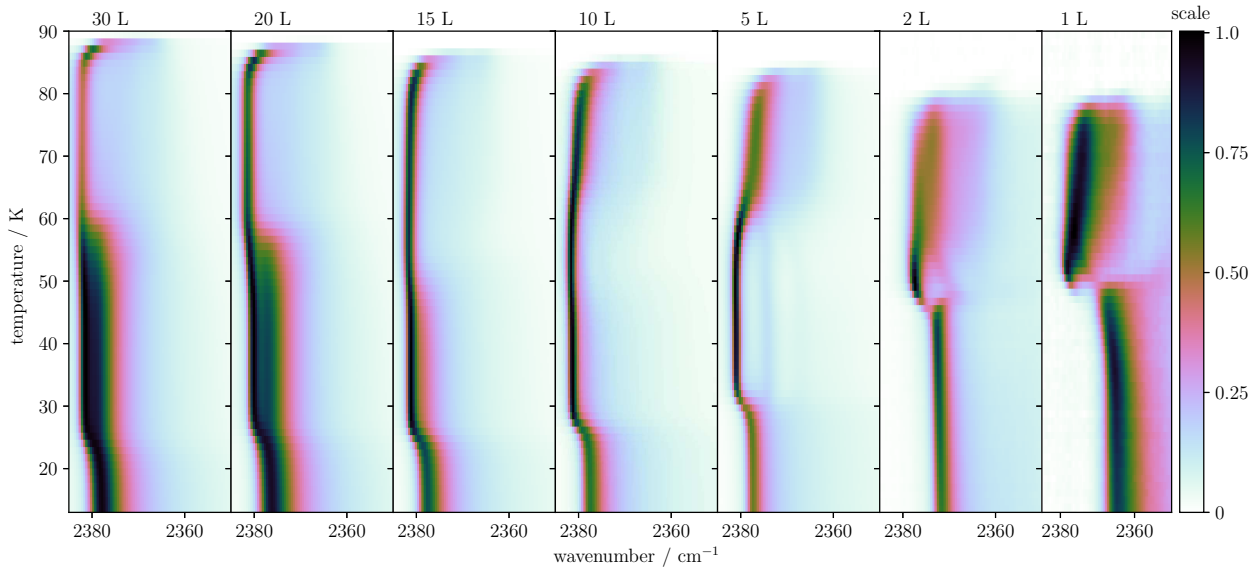


**Figure 1.** Normalized absorption spectra of the CO<sub>2</sub> asymmetrical stretching ( $\nu_3$ ) mode during TPDs. The thickness of the CO<sub>2</sub> ice is marked on the top of each panel. The colorbar scale, on the right side of the figure, shows relative intensity.

In thinner than 5 L ices, the combination modes are too noisy and we don't quantify the *DOC*. There is a dramatic increase in *DOC* between 20 and 30 K for all of the thicknesses, which suggests a significant crystallinity change in this temperature range. We attribute this change to orientational changes of CO<sub>2</sub> molecules in this temperature range: CO<sub>2</sub> molecules reorient and forms intermediate range order (nanocrystals). There are few studies on orientational ordering in CO<sub>2</sub> cubic ice (Torchet et al. 1996; Kuchta & Eppers 1988; Krainyukova & Kuchta 2017). Solid, crystalline CO<sub>2</sub> ice has Pa $\bar{3}$  symmetry in vacuum with four molecules per elementary cell placed along the cubic diagonals. The molecules perform small librations around the diagonal (with the C atom on the diagonal) (Kuchta & Eppers 1988). A recent THEED (Transmission High Energy Electron Diffraction) study on thin ( $\sim 10$  nm) films deposited at  $\sim 65$  K reveals a more complicated rotational motions with the molecular tips (the oxygen atoms) hopping in 24 equivalent positions with a maximum deviation from the diagonal of about 30 degrees and decreasing from 15 to 70 K (Krainyukova & Kuchta 2017).

In the growth of 30 and 20 L ices, although during deposition the sample is at 10 K, gas-phase CO<sub>2</sub> molecules possess room temperature thermal energy, and therefore CO<sub>2</sub> molecules can reorientate right after landing on the surface and form nanocrystals. For thinner ices, it is more difficult to form structures with long-range order. In the extreme case where the ice is very thin (1–2 L), molecules have to diffuse on the substrate surface and form clusters or islands before an intermediate range order (nanocrystalline) structure can be formed. From Fig. 1 it can be seen that for 1 L of CO<sub>2</sub> the transition temperature is at 50 K, which is close to the temperature of diffusion of CO<sub>2</sub> on a compact water ice surface (He et al. 2017). In very thin CO<sub>2</sub> ices, the crystallization temperature is mostly limited by diffusion. The same conclusion should also apply for low concentration of CO<sub>2</sub> mixed in water ice. For ice thicker than 5 L, at higher

temperatures, the *DOC* value increases gradually to unity at about 65 K, and ice becomes almost all crystalline. The emerging  $\nu_3$  TO mode absorption at about 60 K (Fig. 3) also supports the formation of long range order.

#### 4 DISCUSSION

The infrared spectra of pure CO<sub>2</sub> ice deposited at low temperature has been measured previously, e.g. (Sandford & Allamandola 1990; Edridge et al. 2013; Escribano et al. 2013; Isokoski et al. 2013; Gerakines & Hudson 2015); here we compare our results with some of the prior studies. In Isokoski et al. (2013), Fig. 5 shows that the 3000 ML ice grown at 15 K already demonstrates a certain degree of crystallinity and is in the polycrystalline form, in agreement with our results. Between 15 K and 75 K, the degree of crystallinity increases. At 75 K the ice is likely fully crystallized. In Escribano et al. (2013), Fig. 2 shows that the double peak splitting of the bending mode emerges between 20 K and 25 K; this also agrees with our *DOC* vs. temperature curve. However, Fig. 2 in Escribano et al. (2013) shows almost no difference in the bending profile above 25 K until desorption of the ice. This is different from our measurement and Isokoski et al. (2013)'s. It is probably due to the relatively low signal to noise ratio in Escribano et al. (2013); therefore small changes in the absorption profile can not be recognized. Fig. 1 of Escribano et al. (2013) also shows an increase in degree of crystallinity during deposition when the ice is still thin, in agreement with Fig. 5 of our work. In Fig. 6 of Escribano et al. (2013) the 200 ML of CO<sub>2</sub> deposited at 14 K already shows some character of crystalline ice, and this also agrees with our results. In Edridge et al. (2013)'s experiments, CO<sub>2</sub> was deposited at 28 K, which is about the transition temperature from the amorphous phase. Their  $\nu_3$  profiles show a sharp peak at all temperatures during TPD, indicating (poly)crystalline structure.

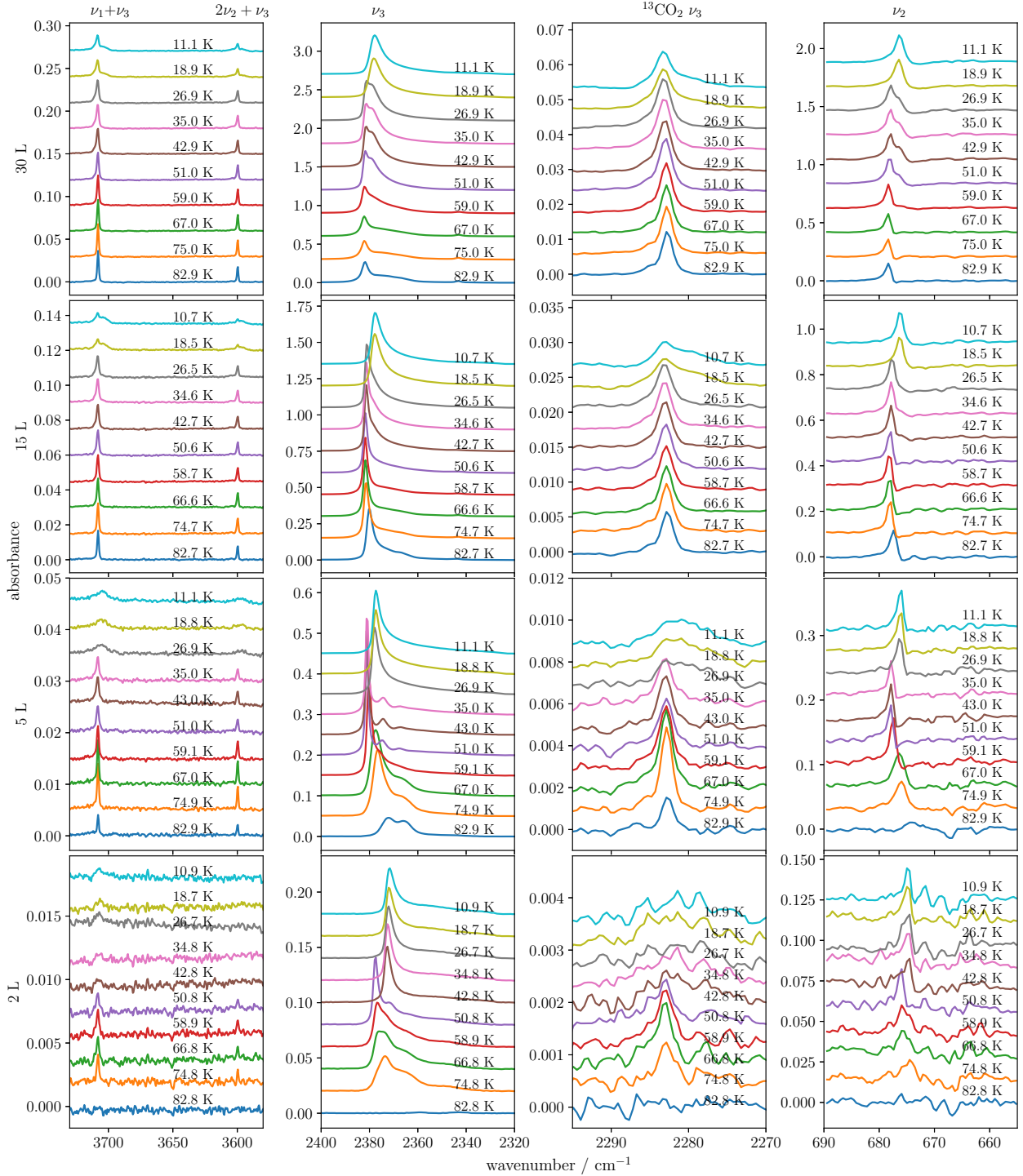


**Figure 2.** RAIRS of 30, 15, 5, and 2 L of CO<sub>2</sub> at selected temperatures. The thickness is labeled on the left side of each row, and the vibrational modes are labeled on the top of each column. Spectra are offset for clarity. The temperature for each curve is also marked. The  $\nu_3$  mode of  $^{13}\text{CO}_2$  (mixed in  $^{12}\text{CO}_2$  with natural abundance) is also shown.

Gerakines & Hudson (2015) also studied the phase of CO<sub>2</sub> ice, and found that their CO<sub>2</sub> ice deposited at a rate of  $0.1 \mu\text{m hr}^{-1}$  (200 times slower than in (Isokoski et al. 2013)) has no sign of crystallization but doubling this deposition rate yields crystalline CO<sub>2</sub>. This disagrees with our work

as well as with Escribano et al. (2013)'s and Isokoski et al. (2013)'s experiments. Given the standard methods used in all these experiments, one is led to conclude that perhaps the explanation lies in the non ultra-high vacuum conditions used in Gerakines & Hudson (2015)'s experiments.

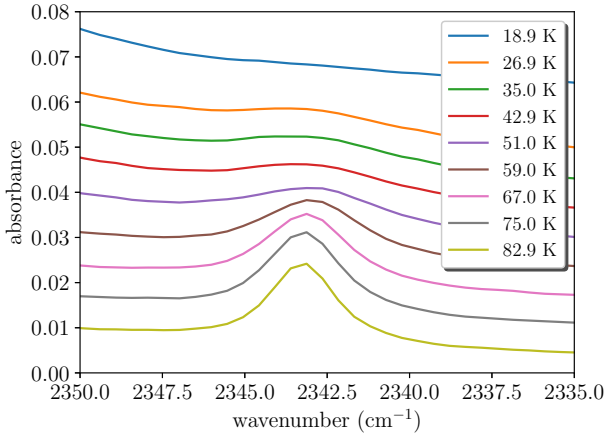


**Figure 3.** Zoom-in of the region of CO<sub>2</sub>  $\nu_3$  TO mode for 30 L CO<sub>2</sub> ice during TPD at selected temperatures.

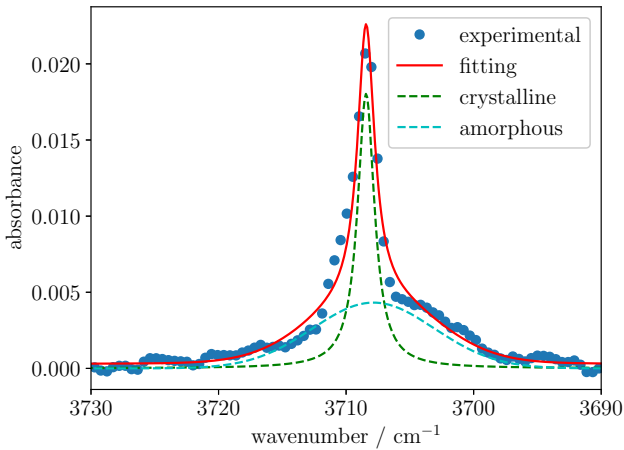


**Figure 4.** A typical fitting of the  $\nu_1 + \nu_3$  combination mode profile using Lorentzian (cyan) and Gaussian (green) distributions.

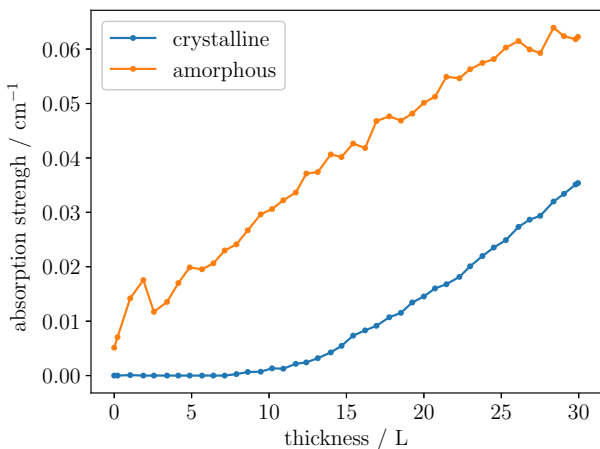


**Figure 5.** The area of Lorentzian (crystalline) and Gaussian (amorphous) components during the deposition of 30 L CO<sub>2</sub> on gold substrate at 10 K.

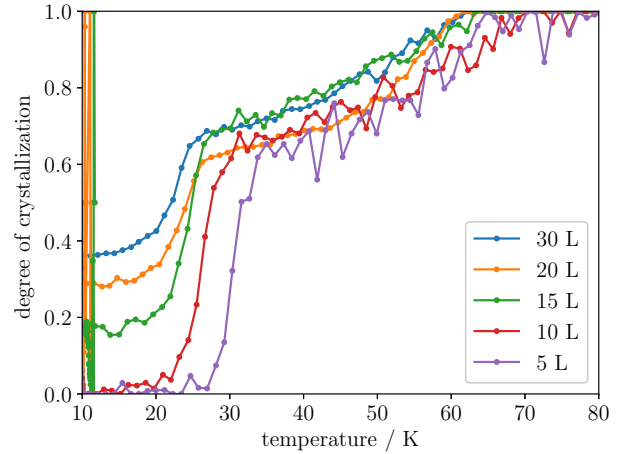


**Figure 6.** Degree of crystallinity (see text) in CO<sub>2</sub> ices of different thickness during TPD.

This discrepancy could be due to contamination from background water in the vacuum chamber during CO<sub>2</sub> deposition. The effect of water in CO<sub>2</sub> ice has been shown to wipe out the sharp features of both  $\nu_3$  and  $\nu_2$  (e.g., [Cooke et al. \(2016\)](#)). A clue that this might be the case resides in [Gerakines & Hudson \(2015\)](#)'s experiments when, by increasing the deposition rate (and, thus, decreasing the deposition time and degree of contamination), the amorphous-like features (broad  $\nu_3$  profile and unresolved  $\nu_2$  splitting) change into crystalline-like ones (sharp  $\nu_3$  and  $\nu_2$  split). To check the effect that water has on the CO<sub>2</sub> ice spectrum, we performed an experiment with a 1:10 mixture of H<sub>2</sub>O:CO<sub>2</sub> at a CO<sub>2</sub> deposition rate of 1 ML/minute. The result is shown in Figure 7. Figure 8 shows the same  $\nu_1 + \nu_3$  mode for pure CO<sub>2</sub> ice. Clearly the mixture with water doesn't show any sign of being crystalline below  $\sim 40$  K, while the pure CO<sub>2</sub> ice shows a sharp peak from 10 K. When heating it, the mixture with water crystallizes. This agrees with [Gerakines & Hudson \(2015\)](#)'s finding that annealing to 70 K crystallizes the ice. Therefore, we suggest that ultrahigh vacuum conditions are important for the study of CO<sub>2</sub> crystallization.

## 5 ASTROPHYSICAL IMPLICATIONS

The segregation and crystallization of CO<sub>2</sub> in ice mantles is a useful probe of the thermal history of ices in dense molecular clouds. While prior works analyzed the double peak splitting of bending profile in efforts to study the segregation and crystallization CO<sub>2</sub> in CO<sub>2</sub>:H<sub>2</sub>O mixtures ([Pontoppidan et al. 2008](#); [Ioppolo et al. 2013](#); [Noble et al. 2013](#)) the splitting profile suffers from the difficulty in separating the double peak feature from CO<sub>2</sub> in other environments. In addition, the shape of the bending mode profile is affected by grain shapes. We propose that the  $\nu_1 + \nu_3$  combination mode profile is a more sensitive probe of pure crystalline CO<sub>2</sub> and, because of its weakness, is not sensitive to dust grain shape effects as the other transitions are ([Keane et al. 2001](#)). Another advantage of the  $\nu_1 + \nu_3$  combination mode profile is that it is similar in both transmission spectra and reflection spectra, therefore can be used

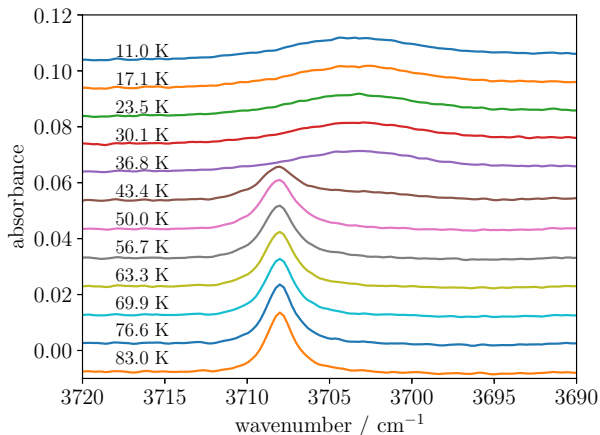


**Figure 7.**  $\nu_1 + \nu_3$  mode of 22 ML of 1:10 H<sub>2</sub>O:CO<sub>2</sub> mixture deposited at 10 K and heated up at 0.1 K/s. The temperature for each spectrum is labeled.

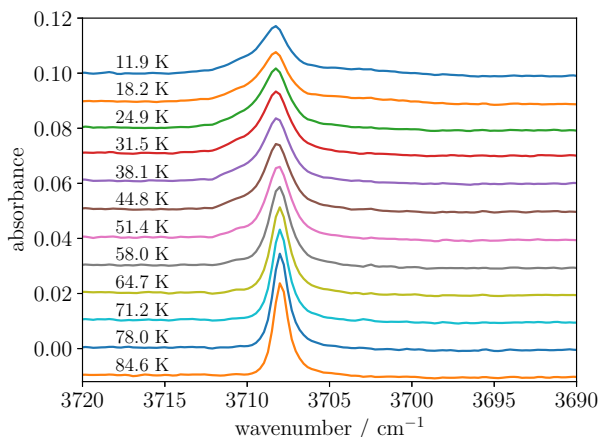


**Figure 8.**  $\nu_1 + \nu_3$  mode of 20 ML of pure CO<sub>2</sub> ice deposited at 10 K and heated up at 0.1 K/s. The temperature for each spectrum is labeled.

by RAIRS measurements and provides more sensitive measurements of ice films with a thickness comparable with the ice mantle. Although very few previous observations of ice mantles provide enough high resolution data covering the combination mode at 2.7  $\mu\text{m}$  (Keane et al. 2001), JWST will provide high quality spectrum data covering this wavelength region. More reliable information of the thermal history of ice mantles can be expected from comparing observational spectra with laboratory measurements.

We also found that there is a dramatic increase in the degree of crystallinity between 20 and 30 K, and we attribute it to orientational ordering of CO<sub>2</sub> molecules. We introduce a new parameter—degree of crystallinity (DOC)—to reliably quantify crystallinity of CO<sub>2</sub> ice. Above 30 K, the CO<sub>2</sub> ice further crystallizes until it becomes fully crystallized at about 65 K. We can separate the formation of pure crystalline CO<sub>2</sub> in ice mantles into two processes: 1) segregation/diffusion of CO<sub>2</sub> to form clusters/islands of CO<sub>2</sub>; 2) the formation of long range order in CO<sub>2</sub> clus-

ters/islands. The latter process becomes efficiently at above 20 K, while the former process has been found to happen at a much higher temperature (He et al. 2017; Öberg et al. 2009; Hodyss et al. 2008). We therefore concludes that the rate limiting process is the segregation of CO<sub>2</sub> from the CO<sub>2</sub>:H<sub>2</sub>O mixture instead of the crystallization process itself. In the case of a low fraction of CO<sub>2</sub> in the mixture, the diffusion of CO<sub>2</sub> on water surface, which has been studied in detail by He et al. (2017), becomes the most important process in the formation of pure crystalline CO<sub>2</sub>.

## ACKNOWLEDGEMENTS

We thank SM Emtiaz, Yujia Huang, and Francis Toriello for technical assistance. This research was supported by NSF Astronomy & Astrophysics Research Grant #1615897.

## REFERENCES

- Baratta G. A., Palumbo M. E., 1998, *JOSAA*, **15**, 3076  
 Bauerecker S., 2005, *Physical Review Letters*, **94**, 033404  
 Berreman D., 1963, *PhRv*, **130**, 2193  
 Boogert A. C. A., et al., 2000, *A&A*, **353**, 349  
 Boogert A. C. A., Gerakines P. A., Whittet D. C. B., 2015, *ARA&A*, **53**, 541  
 Cooke I. R., Fayolle E. C., Öberg K. I., 2016, *ApJ*, **832**, 5  
 Davydov A. S., Sardaryan R. A., 1962, *NucPh*, **37**, 106  
 Edridge J. L., Freimann K., Burke D. J., Brown W. A., 2013, *RSPTA*, **371**, 20110578  
 Ehrenfreund P., Dartois E., Demyk K., D’Hendecourt L., 1998, *A&A*, **339**, L17  
 Ehrenfreund P., et al., 1999, *A&A*, **350**, 240  
 Escribano R. M., Muñoz Caro G. M., Cruz-Díaz G. A., Rodríguez-Lazcano Y., Mate B., 2013, *PNAS*, **110**, 12899  
 Gerakines P. A., Hudson R. L., 2015, *ApJ*, **808**, L40  
 Gerakines P. A., et al., 1999, *ApJ*, **522**, 357  
 He J., Acharyya K., Vidali G., 2016, *ApJ*, **823**, 56  
 He J., Emtiaz S. M., Vidali G., 2017, *ApJ*, **837**, 65  
 Hodyss R., Johnson P. V., Orzechowska G. E., Goguen J. D., Kanik I., 2008, *Icarus*, **194**, 836  
 Ioppolo S., Sangiorgio I., Baratta G. A., Palumbo M. E., 2013, *A&A*, **554**, A34  
 Isokoski K., Poteet C. A., Linnartz H., 2013, *A&A*, **555**, A85  
 Isokoski K., Bossa J.-B., Triemstra T., Linnartz H., 2014, *PCCP*, **16**, 3456  
 Kataeva T. S., Kolomitsova T. D., Shchepkin D. N., Asfin R. E., 2015, *CPL*, **641**, 117  
 Keane J. V., Boogert A. C. A., Tielens A. G. G. M., Ehrenfreund P., Schutte W. A., 2001, *A&A*, **375**, L43  
 Krainyukova N., Kuchta B., 2017, *JLTP*, **187**, 148  
 Kuchta B., Eppers R., 1988, *PhRvB*, **38**, 6265  
 Loerting T., Brazhkin V. V., Morishita T., 2009, *AdChP*, **143**, 29  
 Noble J. A., Fraser H. J., Aikawa Y., Pontoppidan K. M., Sakon I., 2013, *ApJ*, **775**, 85  
 Nummelin A., Whittet D. C. B., Gibb E. L., Gerakines P. A., Chiar J. E., 2001, *ApJ*, **558**, 185  
 Öberg K. I., Fayolle E. C., Cuppen H. M., van Dishoeck E. F., Linnartz H., 2009, *A&A*, **505**, 183  
 Palumbo M. E., Baratta G. A., 2000, *A&A*, **361**, 298  
 Pontoppidan K. M., et al., 2008, *ApJ*, **678**, 1005  
 Price D., 1996, *COSSM*, **1**, 572  
 Sandford S. A., Allamandola L. J., 1990, *ApJ*, **355**, 357  
 Torchet G., de Feraudy M.-F., Boutin A., Fuchs A. H., 1996, *J. Chem. Phys.*, **105**, 3671

Yamagishi M., Kaneda H., Ishihara D., Oyabu S., Onaka T., Shimomishi T., Suzuki T., 2015, *ApJ*, **807**, 29  
de Graauw T., et al., 1996, *A&A*, **315**, L345

This paper has been typeset from a  $\text{\TeX}/\text{\LaTeX}$  file prepared by the author.